

# Breathing dynamics of the Bose polaron in a species-selective harmonic trap

Maxim Pyzh<sup>1,\*</sup> and Peter Schmelcher<sup>1,2,†</sup>

<sup>1</sup>*Zentrum für Optische Quantentechnologien, Universität Hamburg,  
Luruper Chaussee 149, 22761 Hamburg, Germany*

<sup>2</sup>*The Hamburg Centre for Ultrafast Imaging, Universität Hamburg,  
Luruper Chaussee 149, 22761 Hamburg, Germany*

We perform an extensive numerical study on the breathing dynamics of a few-body Bose polaron setup in a one-dimensional species-selective harmonic trap. The dynamics is triggered by a quench of the impurity trap. The excitation of the background majority atoms is mediated via the majority-impurity interaction. The breathing spectrum is obtained for different numbers of majority particles, several values of the majority-component interaction strengths and trap ratios. It is further compared to the breathing spectrum of a particle-balanced few-body Bose-Bose mixture. In particular, for equal post-quench traps the employed protocol allows to couple states of different center-of-mass parity in contrast to species-symmetric trap quenches. Among the participating eigenstates we identify one having odd center-of-mass parity and even global parity. The breathing frequency induced by this state is a monotonically decreasing function of the coupling parameter. Importantly, in order to be observable it requires the entanglement between the species to be taken into account. We demonstrate this by comparing the numerically exact results obtained by means of the Multi-Layer Multi-Configuration Time-Dependent Hartree Method for Mixtures to the ones of a species mean-field ansatz. The entanglement-sensitive breathing frequency persists also for unequal post-quench traps where the center-of-mass cannot be decoupled. Finally, we analyze the impact of parity symmetry on the breathing dynamics by initializing a state of odd global parity. We evidence a striking resemblance to the ground state breathing dynamics.

## I. INTRODUCTION

The polaron concept was introduced quite some time ago by Landau and Pekar [1, 2] to describe the motion of an electron in a crystalline material. The notion of an emerging quasi-particle dressed by low-energy excitations of the underlying medium has vastly expanded since its foundation finding broad applications in different areas of physics such as organic semiconductors, polymers, nanowires, quantum dots and high temperature superconductors [3–5]. Since the advent of ultracold gases [6, 7] a promising experimental platform has emerged allowing to investigate fundamental many-body quantum processes [8] with an exquisite tunability of the underlying interactions and trapping geometries. In particular, the ability to combine different species [9] and the precise control over the number of particles [10] made it possible to experimentally prepare an impurity in a many-body environment of bosons [11–16] or fermions [17–21] leading to what is nowadays termed Bose [22] and Fermi polaron [23, 24], respectively. A mapping to the Fröhlich Hamiltonian [25] for the polaron problem can be established while all the Hamiltonian parameters can be addressed individually. The tunability of interactions via Feshbach resonances [26, 27] provides access to highly correlated and entangled regimes challenging the theorists to go beyond the weak coupling Fröhlich paradigm [28–34].

The correlations are in particular enhanced in quasi-one-dimensional (1D) systems [35]. A comparatively

tight transverse confinement freezes the perpendicular motion of particles and additionally affects the effective 1D interactions known as confinement-induced resonances [36–38]. A prominent example of a strongly correlated 1D system is the Tonks-Girardeau gas [39–41]. In contrast to higher dimensions, where a lower particle density implies weaker correlations, in 1D lower densities lead to stronger interactions. It makes the study of low-density few-body systems of particular interest triggering significant research efforts [42–46]. At the same time this represents a great challenge requiring sophisticated numerical techniques able to account for all the relevant correlations when characterizing the static properties or the many-body dynamics, such as the Density Matrix Renormalization Group (DMRG) [47] or the Multi-Layer Multi-Configuration Time-Dependent Hartree Method for Bosons and Fermions (ML-MCTDHF) [48]. In species-selective trapping geometries [12, 49, 50] the inhomogeneity of the medium and the localization length of the impurity impact significantly the degree of correlations [51–53] opening interesting perspectives but requiring also new approaches since the translation symmetry is broken making the well established technique, the Lee-Low-Pines transformation [54], inapplicable.

In this work we investigate the low-energy breathing dynamics of a 1D few-body Bose polaron in a species-selective parabolic confinement. Elementary collective excitations [12, 17, 55–59] are of fundamental importance to understand the dynamical response of a physical system subject to a weak perturbation in terms of excited eigenstates and the respective eigenenergies. Here, we focus on the so-called breathing modes [60]. On account of their strong sensitivity to the system’s parameters such as

\* mpyzh@physnet.uni-hamburg.de

† pschmelc@physnet.uni-hamburg.de

interactions, trap geometry and spin statistics, they have been established as a reliable diagnostic tool to access the ground state properties of a system [61], for precision measurements of the scattering lengths [56] and even as a sensitive test of the equation of state at unitarity [62, 63]. We make use of the species-selective trapping potentials to compress only the trap of the impurity and monitor the response in the majority component owing to the inter-component coupling. For different system parameters we classify the breathing modes according to their relative amplitude in the Fourier power spectrum obtained by applying a Compressed Sensing (CS) [64] algorithm to breathing observables and study the role of entanglement and parity symmetry on breathing response. We identify a unique mode whose frequency is a monotonically decreasing function of the majority-impurity interaction while its presence relies on the entanglement between the impurity and the majority component.

This work is structured as follows. In Section II we introduce our setup and Hamiltonian. The numerical approach is discussed Section III A. We use ML-MCTDHX for state initialization, subsequent dynamics and evaluation of breathing observables. The oscillation frequencies are extracted by means of a CS algorithm outlined in Section III B. The results presented in Section IV are categorized in four subtopics: an overview of breathing modes in a particle-balanced few-body Bose-Bose mixture [65] (Section IV A) for later reference, the breathing spectra in the current Bose polaron setup for different majority-component interactions and particle number ratio (Section IV B), the impact of impurity localization length (Section IV C) and, finally, the role of global parity symmetry for the breathing response (Section IV D). In Section V we summarize the most important insights.

## II. SETUP AND HAMILTONIAN

We consider a few-body mixture of two bosonic components. A component  $\sigma \in \{A, B\}$  contains  $N_\sigma$  particles of mass  $m_\sigma$ , which experience a quasi one-dimensional parabolic confinement with trap frequency  $\omega_\sigma$  and interact internally via contact pseudo interaction of strength  $g_\sigma$ . The components are coupled via an inter-species contact interaction of strength  $g_{AB}$ . We assume equal masses and introduce harmonic units of component A as our natural units, i.e.,  $l_A = \sqrt{\hbar/m\omega_A}$  for length,  $\hbar\omega_A$  for energy and  $1/\omega_A$  for time. The corresponding Hamilto-

nian reads as follows:

$$\begin{aligned} H &= H_A + H_B + H_{AB} = \\ &= \sum_{i=1}^{N_A} \left( -\frac{1}{2} \frac{\partial^2}{\partial x_i^2} + \frac{1}{2} x_i^2 \right) + g_A \sum_{i<j}^{N_A} \delta(x_i - x_j) + \\ &+ \sum_{i=1}^{N_B} \left( -\frac{1}{2} \frac{\partial^2}{\partial y_i^2} + \frac{1}{2} \eta^2 y_i^2 \right) + g_B \sum_{i<j}^{N_B} \delta(y_i - y_j) + \\ &+ g_{AB} \sum_{i=1}^{N_A} \sum_{j=1}^{N_B} \delta(x_i - y_j), \end{aligned} \quad (1)$$

where  $x_i$  ( $y_i$ ) denotes the position of the  $i$ th particle in the A (B) component.

The A component is referred to as the majority species. It has  $N_A \in \{5, 10\}$  particles. The B component consists of a single particle,  $N_B = 1$ , and we call it the impurity. The majority-component is either non-interacting ( $g_A = 0$ ) or features a weakly attractive/repulsive interaction ( $g_A = \pm 0.5$ ). The majority-impurity coupling covers values from weakly attractive to intermediate repulsive  $g_{AB} \in [-0.5, 2.0]$ . The trap ratio covers cases of equal traps ( $\eta = 1$ ), a 'broad' impurity ( $\eta = 0.51$ ) and a 'narrow' impurity ( $\eta = 4$ ).

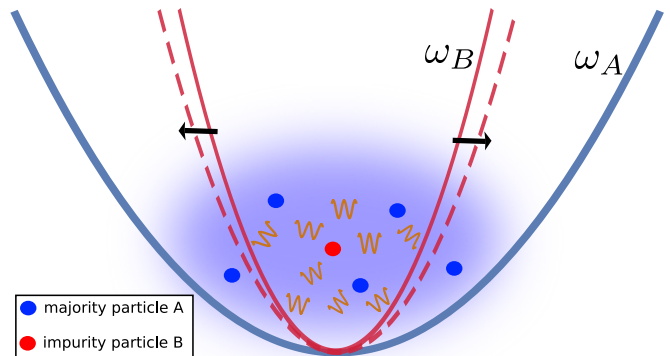


Figure 1. The impurity (species B indicated by a red circle) in a harmonic trap (red solid line) is immersed in a cloud of majority atoms (species A indicated by a blue ellipse) subject to a different parabolic confinement (blue solid line). The breathing dynamics is initiated by quenching the trap of the impurity (red dashed line) inducing thereby excitations (orange waves) in the composite system via the majority-impurity interaction.

The Hamiltonian Eq. (1) possesses a global reflection symmetry, corresponding to a map  $x_i \mapsto -x_i$  and  $y_j \mapsto -y_j$  for all  $i, j$ . The eigenstates can be thus partitioned into two decoupled subspaces of even and odd global parity. As our initial state we take the lowest energy eigenstate from either of the two subspaces. To initiate the breathing dynamics we slightly relax the trap of the impurity from  $1.05\eta$  to  $\eta$ . The majority species is set in breathing motion indirectly via the coupling to the impurity.

The breathing motion can be monitored in the one-body densities  $\rho_1^\sigma(z, t)$  as their widths expand and con-

tract periodically in time. Alternatively, one can analyze the time-evolution of the corresponding breathing observables  $\langle \hat{O} \rangle_t$  with  $\hat{O} = \sum_i \hat{x}_i^2$  for the majority species and  $\hat{O} = \hat{y}^2$  for the impurity. Such an oscillatory motion is usually composed of multiple contributions with distinct amplitudes  $d_n$  and frequencies  $\Omega_n$ , i.e.,  $\langle \hat{O} \rangle_t = \sum_n d_n e^{-i\Omega_n t}$ . Each of the oscillatory contributions in  $\langle \hat{O} \rangle_t$  will be referred to as a *breathing mode* characterized by a distinct frequency. The origin of the breathing modes can be expressed in terms of system's eigenstates and related eigenenergies as follows. Upon a quench, several eigenstates  $|\psi_n\rangle$  of the post-quench Hamiltonian  $H$  with energy  $E_n$  become populated depending on the overlap  $c_n$  with the initial state  $|\Psi(t_0)\rangle$ , i.e.,  $c_n = \langle \psi_n | \Psi(t_0) \rangle$ . The time signal  $\langle \hat{O} \rangle_t = \sum_{n,m} c_m^* c_n \langle \psi_m | \hat{O} | \psi_n \rangle e^{-i\Omega_{n,m} t}$  oscillates with frequencies  $\Omega_{n,m} = E_n - E_m$  for populated eigenstates  $c_n c_m \neq 0$  as long as the transition matrix elements  $\langle \psi_n | \hat{O} | \psi_m \rangle = O_{nm}$  are non-zero. Given a weak perturbation, we expect the lowest energy eigenstate of even (odd) parity  $|\psi_{\text{ref}}\rangle$  to have the largest overlap with the even (odd) parity initial state  $|\Psi(t_0)\rangle$ . For that reason, the major part of frequencies contained in the breathing observable  $\langle \hat{O} \rangle_t$  are energy gaps between any of the populated eigenstates and the reference eigenstate, i.e.,  $\Omega_n = E_n - E_{\text{ref}}$ . Oscillations among any different combination of eigenstates are of minor amplitude, so we don't focus on them by setting a suitable amplitude threshold. For that reason, when we refer to an eigenstate of a breathing mode we mean the eigenstate responsible for this mode while the reference state  $|\psi_{\text{ref}}\rangle$  is usually clear within the context, unless we state otherwise.

For  $\eta = 1$  the center-of-mass coordinate can be decoupled by employing a transformation to the center-of-mass and internal coordinates such as Jacobi coordinates. This provides an exact quantum number of the 'free' center-of-mass harmonic oscillator. At first glance, it is appealing to operate in the center-of-mass frame. However, the two-body interactions are mapped to higher order interaction terms while the exchange symmetry for indistinguishable majority coordinates in the laboratory frame becomes a set of complex rules in the center-of-mass frame. Furthermore, for  $\eta \neq 1$  the center-of-mass cannot be separated. Hence, we employ the laboratory frame.

### III. COMPUTATIONAL APPROACH AND ANALYSIS

In this work we use the Multi-Layer Multi-Configuration Time-Dependent Hartree Method for Mixtures to initialize a system in its ground state by means of relaxation, i.e., propagation in imaginary time, for the state evolution following a trap quench of the impurity and to evaluate the expectation values of breathing observables for each species as a function of time. We outline the major idea of the method in Section III A along with the wave function ansatz for the system at hand. We then apply a Compressed Sensing algorithm to re-

tain the frequencies from those observables. In view of the fact that CS relies on the sparsity condition in the Fourier space, it is not used as a standard tool for frequency extraction from a time signal. In Section III B we discuss advantages of this method in the current application as compared to a straightforward Fourier transformation. In order to be self-contained we also provide the implementation details.

#### A. ML-MCTDHX

To prepare the initial state  $|\Psi(t_0)\rangle$  and to perform the subsequent time evolution  $|\Psi(t)\rangle = e^{-iHt} |\Psi(t_0)\rangle$  with the time-independent Hamiltonian  $H$  from Eq. (1) we employ the *Multi-Layer Multi-Configuration Time-Dependent Hartree Method for Mixtures* of indistinguishable particles, for short ML-X [48, 66, 67]. The core idea behind ML-X is to expand the many-body wavefunction in a properly symmetrized product state basis, the so-called Fock states, such that the underlying single-particle functions (SPFs) are *time-dependent*. These are variationally optimized during the time evolution to provide a more 'compact' description compared to Fock states composed of time-independent SPFs. Compact means that in general much less SPFs are required reducing thus the Fock space dimension while retaining a similar degree of accuracy.

As the system evolves, the many-body state travels through different subspaces of the complete Hilbert space. If the Fock basis is fixed, in general a large set of SPFs is required to cover all the relevant subspaces. Many configurations become 'actively' populated during the time-evolution, though not necessarily all of them at the same time with a fraction staying or becoming inactive. Even when all of Fock states are populated, we may rotate the basis by choosing a different set of SPFs until, eventually, we end up with a more compact representation. Given a truncated Fock space, ML-X rotates the basis vectors such as to find the best possible representation of the exact many-body state at each instant of time. In other words, it looks for the current 'active' subspace. Once the truncated variationally evolving Fock-space becomes large enough to contain the (major part of) 'active' subspace, the representation of  $|\Psi(t)\rangle$  given by ML-X is considered optimal.

The underlying wave function ansatz for the Bose polaron problem belonging to Eq. (1) is expanded in two layers (Multi-Layer):

$$|\Psi(t)\rangle = \sum_{i=1}^S \sqrt{\lambda_i(t)} |\Psi_i^A(t)\rangle \otimes |\Psi_i^B(t)\rangle, \quad (2)$$

$$|\Psi_i^\sigma(t)\rangle = \sum_{\vec{n}^\sigma | N_\sigma} C_{i,\vec{n}^\sigma}(t) |\vec{n}^\sigma(t)\rangle. \quad (3)$$

In the first step, see Eq. (2), the majority and impurity degrees of freedom,  $x_i$  and  $y$  respectively, are sep-

arated and assigned to  $S \in \mathbb{N}$  time-dependent species wave-functions  $|\Psi_i^\sigma(t)\rangle$ . The sum of product form is very convenient as it makes evident the entanglement between the two components. The time-dependent weights  $\lambda_i(t)$  are normalized  $\sum_i^S \lambda_i(t) = 1$  and sorted in descending order. A composite system with  $\lambda_1(t) \approx 1$  is considered disentangled. Assuming  $S = 1$  in the expansion is called a species mean-field approximation. In the second step, see Eq. (3), the species wave-functions belonging to the same component are expanded in the same Fock-state basis  $|\vec{n}^\sigma(t)\rangle$  with time-dependent coefficients  $C_{i,\vec{n}^\sigma}(t)$ . The time-dependence of number states is meant implicitly through the time-dependence of  $s_\sigma \in \mathbb{N}$  underlying SPFs  $\varphi_j^\sigma(t)$  which are represented using a harmonic discrete variable representation (DVR) [68]. The notation  $\vec{n}^\sigma|N_\sigma$  denotes particle number conservation, i.e.,  $\sum_i^{s_\sigma} n_i^\sigma = N_\sigma$ . Finally, by applying the Dirac-Frenkel variational principle [69] the equations of motion for  $\lambda_i$ ,  $C_{i,\vec{n}^\sigma}$  and  $\varphi_j^\sigma$  are obtained. The convergence of ML-X is controlled via  $S$ ,  $s_\sigma$  and the number of DVR grid points. We use  $S = s_\sigma = 8$  for  $N_A = 5$  and  $S = s_\sigma = 6$  for  $N_A = 10$ . The DVR grid spans an interval  $[-6, 6]$  and we choose 151 DVR grid points.

## B. Compressed Sensing Analysis

In this work, we aim to extract frequencies  $\Omega_{n,m} = E_n - E_m$  of system's excitations where  $E_n$  denotes the eigenenergy of the  $n$ -th eigenvector  $|\psi_n\rangle$  of  $H$ . Any physical observable  $\hat{O}$  carries information about excited eigenstates  $\langle \hat{O} \rangle_t = \sum_{n,m} c_m^* c_n \langle \psi_m | \hat{O} | \psi_n \rangle e^{-i\Omega_{n,m}t}$ , as long as the transition matrix elements  $\langle \psi_m | \hat{O} | \psi_n \rangle$  are non-zero and the corresponding eigenstates are initially populated  $c_n c_m \neq 0$  where  $c_n = \langle \psi_n | \Psi(t_0) \rangle$ . We perform a sampling of breathing observables with a uniform rate  $\Delta t$  over an interval  $[0, T]$  containing  $T/\Delta t + 1 = N_t$  points. It gives us a finite time signal  $\mathbf{f} \in \mathbb{R}^{N_t}$  with components  $f_j$  of discrete variable  $t_j \in \mathbb{R}$ , i.e.,  $f_j = f(t_j) = f(\Delta t \cdot j)$  with integer index  $j \in [0, N_t - 1] \subset \mathbb{N}_0$ .

A straightforward way to retain the frequencies contained in  $\mathbf{f}$  is to perform a discrete Fourier transformation (DFT), expressed as a linear map  $\mathbf{A}\mathbf{f} = \mathbf{g}$  with a square matrix  $\mathbf{A} \in \mathbb{C}^{N_t \times N_\omega}$  and signal's representation in the frequency domain  $\mathbf{g} \in \mathbb{C}^{N_\omega}$ . The latter is characterized by frequency spacing  $\Delta\omega$  and cut-off frequency  $\omega_{cut}$ , i.e., it has components  $g_j = g(\omega_j) = g(\Delta\omega \cdot j)$  of discrete variable  $\omega_j \in \mathbb{R}$  and for odd (even)  $N_\omega = N_t$  number of points spans an open (closed) interval with endpoints  $-\omega_{cut}/2$  and  $\omega_{cut}/2$ .

The sampling parameters of time and frequency domain are interrelated. Thus, the sampling time  $T$  determines the frequency spacing  $\Delta\omega = 2\pi/T$ , while the sampling rate  $\Delta t$  determines the Nyquist frequency  $\omega_{cut} = \pi/\Delta t$ . In principle, frequencies can be retained with arbitrary resolution, if sampled long enough, while highly oscillatory components require a finer sampling rate. In

practice, there are technical limitations such as generation, storage and processing of data. Given a complex system such as ours, data generation becomes a time-consuming factor making a good resolution in frequency domain out of reach.

In order to overcome this obstacle, some prior information about signal's properties might become useful. Since the system is perturbed weakly, we expect only the low-energy excitations to be of relevance for the underlying dynamics. In particular, we expect  $\mathbf{g}$  to be sparse with major components located in the low-frequency region.

With this prior knowledge *compressed sensing* (CS) allows to retain the frequencies with a very high resolution while keeping the simulation time with ML-X reasonably small. To this end, we formulate our problem as finding the vector  $\mathbf{g}$  satisfying the inverse DFT condition, i.e.,  $\mathbf{f} = \mathbf{A}^\dagger \mathbf{g}$ . However,  $\mathbf{A}^\dagger \in \mathbb{C}^{N_t \times N_\omega}$  is now a rectangular matrix with  $N_\omega \gg N_t$  and  $\mathbf{g} \in \mathbb{C}^{N_\omega}$  resulting in an underdetermined system of equations. Here,  $\mathbf{A}^\dagger$  is a sub-matrix of the inverse square DFT matrix  $\mathbf{A}^\dagger \in \mathbb{C}^{N_\omega \times N_\omega}$ , with the last  $N_\omega - N_t$  rows being removed. Importantly, the number of columns  $N_\omega$  and thus the frequency spacing  $\Delta\omega$  can be chosen independently of the simulation time  $T$ . Intuitively, this implies that  $\mathbf{g}$  has been generated by a signal extended over a larger region  $T' > T$  than the current one  $\mathbf{f}$ , though the information contained beyond  $T$  is considered redundant given the priors underlying the evolution.

In order to find a sparse solution to a linear ill-posed inverse problem we formulate it as  $\ell_1$ -norm penalized least-squares minimization task known as *basis pursuit denoising* (BPDN) [70]:

$$\min_{\mathbf{g}} \frac{1}{2} \|\mathbf{f} - \mathbf{A}^\dagger \mathbf{g}\|_2^2 + \lambda \|\mathbf{g}\|_1, \quad (4)$$

where  $\|\mathbf{x}\|_p = (\sum_i |x_i|^p)^{1/p}$  while the penalty term  $\lambda \geq 0$  controls the trade-off between the sparsity of the solution and the constraint violation in the presence of noisy signal  $\mathbf{f}$ . We use the Least Angle Regression (LARS) [71] minimization algorithm to solve Eq. (4) and perform a mean-normalization of the signal  $\mathbf{f} \rightarrow \tilde{\mathbf{f}} = (\mathbf{f} - \bar{\mathbf{f}})/\|\mathbf{f}\|_1$  beforehand. The employed implementation requires real inputs in Eq. (4). Real  $\mathbf{f}$  implies hermitian  $\mathbf{g}$  and we use this symmetry to reformulate  $\mathbf{g}$  as a real vector:  $\mathbf{g} \rightarrow \tilde{\mathbf{g}} \in \mathbb{R}^{2N_\omega} = (\text{Re}(\mathbf{g}), \text{Im}(\mathbf{g}))$ . Correspondingly, the inverse Fourier matrix  $\mathbf{A}^\dagger \rightarrow \mathbf{M} \in \mathbb{R}^{N_t \times 2N_\omega} = (\mathbf{C}, \mathbf{D})$  is now composed of two real sub-matrices  $\mathbf{C} \in \mathbb{R}^{N_t \times N_\omega}$  with components  $c_{i,j} = \cos(\epsilon ij)$  and  $\mathbf{D} \in \mathbb{R}^{N_t \times N_\omega}$  with components  $d_{i,j} = \sin(\epsilon ij)$  where  $\epsilon = \Delta t \Delta \omega$ . The ML-X time-domain parameters are chosen as  $T = 40$  and  $\Delta t = 0.05$ , whereas the CS frequency-domain parameters are  $\omega_{cut} = 20$  and  $\Delta\omega = 0.01$ .<sup>1</sup>

<sup>1</sup> We remark that similar resolution with DFT can be obtained with  $T \approx 600$ .

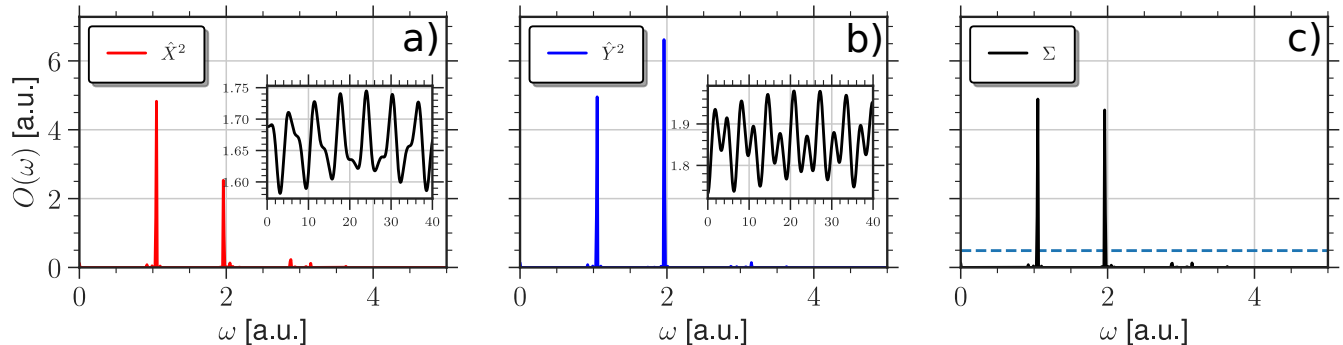


Figure 2. Fourier power spectrum  $X^2(\omega)$  (a) and  $Y^2(\omega)$  (b) obtained by applying a Compressed Sensing algorithm to the expectation values of the breathing observables  $\langle \sum_i \hat{x}_i^2 \rangle_t$  and  $\langle \hat{y}^2 \rangle_t$  (insets) evaluated w.r.t. a dynamical state  $|\Psi(t)\rangle$  obtained by the Multi-Layer Multi-Configuration Time-Dependent Hartree Method for Mixtures. In the averaged power spectrum  $\Sigma(\omega)$  (c) the blue dashed line indicates a threshold magnitude and only frequencies above it are accounted for in Section IV (see text). The physical parameters are  $\eta = 1$ ,  $N_A = 5$ ,  $N_B = 1$ ,  $g_{AB} = 2.0$ ,  $g_A = 0$  (see Section II) and the Compressing Sensing parameters are  $T = 40$ ,  $\Delta t = 0.1$ ,  $\omega_{cut} = 20$  and  $\Delta\omega = 0.01$  (see Section III B).

As input time signals  $\mathbf{f}$  we use the expectation values of breathing observables  $\sum_i \hat{x}_i^2$  for the majority species and  $\hat{y}^2$  for the impurity evaluated w.r.t. the dynamical state  $|\Psi(t)\rangle$  obtained by ML-X. We apply the CS algorithm to obtain the corresponding vector  $\tilde{\mathbf{g}}$ . Then, we map  $\tilde{\mathbf{g}}$  back to  $\mathbf{g}$  and convert complex values into amplitudes, i.e.,  $g_j \rightarrow |Re(g_j) + Im(g_j)|$ . The final vector we call a Fourier power spectrum and label it as  $X^2(\omega)$  for the majority component and  $Y^2(\omega)$  for the impurity. Finally, for a fixed set of physical parameter values we construct an averaged power spectrum  $\Sigma = (X^2 + Y^2)/2$ . An example is shown in Fig. 2. Each frequency is classified as being of a majority type (red), an impurity type (blue) or of a mixed type depending on the relative weights of  $X^2$  and  $Y^2$  in  $\Sigma$ . These are encoded in subsequent figures as a pie chart of two colors for each breathing frequency. Additionally, we use the transparency to indicate the magnitude of participating breathing modes relative to the most relevant mode of amplitude  $\max(\Sigma) = \Sigma_{\max}$  such that faded colors imply less relevant modes. Frequencies with a contribution below  $\Sigma_{\max}/10$  are discarded. This amounts to neglecting i) low-amplitude oscillations among any two eigenstates not involving the reference eigenstate with the largest population, and ii) numerically introduced 'phantom' peaks which are also of minor amplitude.

#### IV. RESULTS

First, in Section IV A we summarize results concerning the breathing dynamics of a single particle, a single-component condensate, two distinguishable particles and a particle-balanced Bose-Bose mixture. This will provide us with useful insights for the interpretation of breathing modes unraveled in the Bose polaron setup being the subject of Section IV B. In Section IV C we investigate the impact of the trap ratio  $\eta$  on the breathing spectrum

accounting for two cases: a 'broad' ( $\eta < 1$ ) and a 'narrow' ( $\eta > 1$ ) impurity. Finally, in Section IV D we study the breathing response of the first excited state having odd parity and contrast it to the response of the ground state which is of even parity.

In the following, when all interactions are zero we employ a notation  $|\vec{n}\rangle = |n_1, n_2, \dots\rangle$  to denote  $n_i$  particles occupying the  $i$ -th orbital of a single-particle quantum harmonic oscillator. It is not to be confused with permanents introduced in Section III A where the orbitals are variationally optimal at each time instant. We also drop the redundant zeroes in the vector tail once all the particles have been accounted for, i.e.,  $\sum_i n_i = N$ . The notation  $|\vec{n}^A\rangle \otimes |\vec{n}^B\rangle$  denotes a product state for the two components. Note that for unequal traps ( $\eta \neq 1$ ) the orbitals for each species are different.

##### A. Bose-Bose mixture

The breathing mode frequency of a single particle confined in a parabolic trap of frequency  $\omega$  is known to be  $\Omega = 2\omega$ , corresponding to an excitation by two energy quanta  $|0, 0, 1\rangle$  w.r.t. the harmonic oscillator basis. An ensemble of  $N$  non-interacting ( $g = 0$ ) bosonic particles introduces an additional eigenstate of the same excitation energy  $2\omega$ , namely a two-particle excitation  $|N - 2, 2\rangle$  being degenerate with  $|N - 1, 0, 1\rangle$ . For interacting particles the degeneracy is lifted. The frequency of one mode remains constant for any  $g$  and relates to the center-of-mass (CM) breathing motion. The frequency of the other mode is highly sensitive to a variation of  $g$  and characterizes the relative motion of particles [72]. A mean-field ansatz for the breathing dynamics, being a single-particle picture, is able to recover only the interaction-sensitive breathing frequency, though with quantitative deviations as compared to an exact solution, especially at sizable interactions.

Two distinguishable non-interacting particles  $A$  and  $B$  confined in the same harmonic trap ( $\eta = 1$ ) have three eigenstates with excitation energy  $2\omega$ : a single particle excitation by two energy quanta in either of the components, i.e.,  $|0, 0, 1\rangle \otimes |1\rangle$  and  $|1\rangle \otimes |0, 0, 1\rangle$ , as well as a two-particle-excitation  $|0, 1\rangle \otimes |0, 1\rangle$ . The latter can be also interpreted as a simultaneous excitation of a sloshing mode in each species. When the coupling between the particles becomes non-zero, the degenerate manifold splits giving rise to one constant frequency mode ( $\Omega = 2\omega$ ) and two modes with an interaction sensitive oscillation period (not shown). One of the latter two modes features a frequency which is a convex function of  $g_{AB}$ . The other mode is remarkable in the sense that the energy of the involved excited eigenstate is independent of the interaction while the ground state energy (reference eigenstate) grows with increasing  $g_{AB}$ . As a result, the corresponding breathing mode frequency is a monotonically decreasing function of the coupling  $g_{AB}$ . It saturates to a sloshing mode frequency  $\Omega = \omega$  at very large positive couplings. Thus, distinguishability allows for an additional breathing mode. A species mean-field ansatz can identify two coupling sensitive breathing frequencies though neither of the exact modes will be matched quantitatively for all interactions. In particular, the monotonically decreasing frequency is not accounted for implying the relevance of entanglement in multi-component mixtures.

A non-interacting two-component mixture features in total five eigenstates which are two energy quanta above the ground state: two single-particle excitation states  $|N_A - 1, 0, 1\rangle \otimes |N_B\rangle$  and  $|N_A\rangle \otimes |N_B - 1, 0, 1\rangle$ , two states having two indistinguishable particles excited  $|N_A - 2, 2\rangle \otimes |N_B\rangle$  and  $|N_A\rangle \otimes |N_B - 2, 2\rangle$ , and, finally, a state where one particle in each component is excited  $|N_A - 1, 1\rangle \otimes |N_B - 1, 1\rangle$ . The interactions will (partially) break this manifold of degenerate eigenstates. Each of these states, once populated in the initialization step, will induce a breathing oscillation of a characteristic frequency. Together they represent a first order breathing manifold. To get an insight how the respective frequencies behave depending on the system's interactions we briefly summarize and complement the results obtained in [65].

In [65], each component consists of two particles trapped within the same parabolic confinement  $\eta = 1$ . Both components experience a sudden but weak trap quench of the same magnitude and the system's response is studied for different intra- and inter-component interaction strengths. Importantly, the CM motion decouples while the quench operator prevents transitions among eigenstates possessing different CM parity. Four breathing mode frequencies have been identified and analyzed. One of them is constant  $\Omega_{CM} = 2$ . The remaining three are sensitive to interactions and have been labeled  $\Omega_+$ ,  $\Omega_-$  ( $\Omega_A$ ,  $\Omega_B$ ) for species-(anti)symmetric parameter choice, i.e.,  $g_A = g_B$  ( $g_A \neq g_B$ ), and  $\Omega_{AB}$ , all related to the relative motion of the particles.

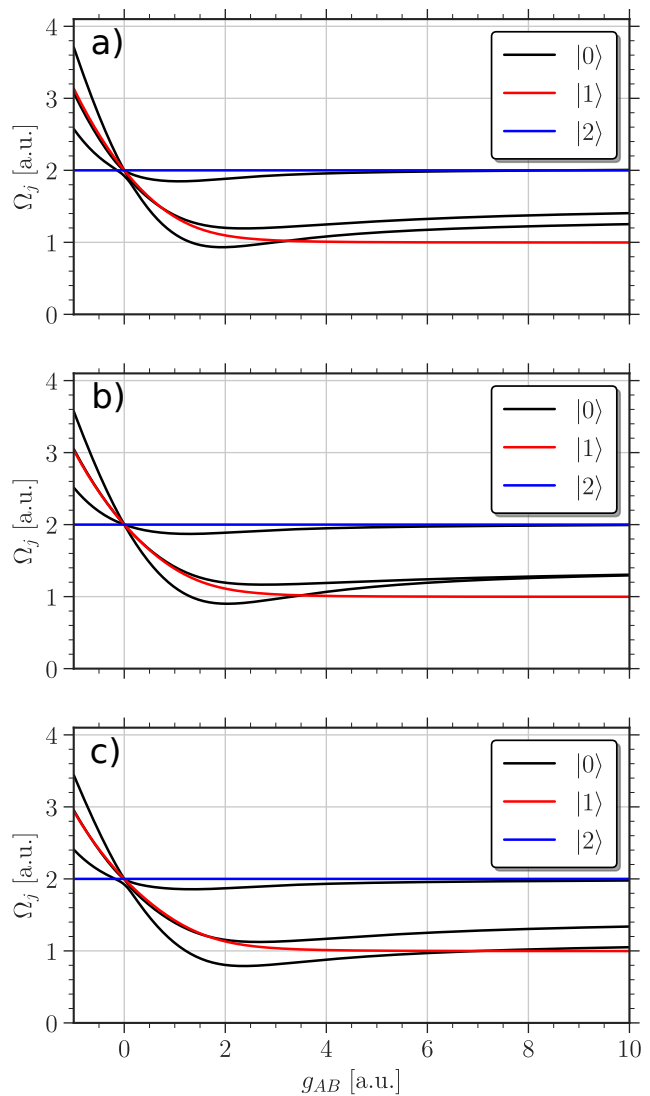


Figure 3. Breathing mode frequencies  $\Omega_j = E_j - E_0$  (w.r.t. the ground state  $|E_0\rangle$ ) of a few-body bosonic mixture  $N_A = 2$  and  $N_B = 2$  as a function of the inter-component coupling  $g_{AB}$  at equal trapping frequency ratio  $\eta = 1$ , intra-component interaction strength  $g_A = 0$  for the first component and a)  $g_B = -0.5$ , b)  $g_B = 0$ , c)  $g_B = 0.5$  for the second component. Whether the modes are actually excited depends on the quench protocol. Different colors refer to the center-of-mass (CM) quantum number in the eigenstate  $|E_j\rangle$ . The CM is a decoupled degree of freedom in this harmonic confinement.

In Fig. 3 the breathing frequencies of the above-mentioned modes are displayed as a function of the inter-component coupling  $g_{AB}$  for three different intra-component interaction values  $g_B$  (subfigures a-c), assuming  $g_A = 0$ . The curve colors encode the CM quantum number of the responsible eigenstates  $|E_j\rangle$ , while the reference state  $|E_{\text{ref}}\rangle$  is the ground state  $|E_0\rangle$  of even CM parity. The blue curve is the  $\Omega_{CM}$  mode and is indeed constant for any values  $g_A$ ,  $g_B$  and  $g_{AB}$ . The three black curves are the above-mentioned interaction-

sensitive relative modes. All of them have a common signature, namely a single minimum though at different values of  $g_{AB}$  depending on the choice of intra-component interactions. The one with the largest frequency is the  $\Omega_{AB}$  mode. It is quite shallow, weakly affected by intra-component interactions and degenerates with  $\Omega_{CM}$  at strong coupling  $g_{AB}$ . The two lower ones are very sensitive to intra-component interactions and, depending on the presence of the species-exchange symmetry<sup>2</sup>, experience a bending in the vicinity of avoided crossings (Fig. 3a and Fig. 3c at  $g_{AB} \approx 0$ ). Finally, the red curve represents a mode caused by an eigenstate of odd CM parity but even global parity. We observe a monotonous decrease of the mode frequency with increasing coupling  $g_{AB}$  until it energetically separates from one of the relative modes at  $g_{AB} \approx 1$  and, finally, saturates to a value of 1.0 at  $g_{AB} \geq 4$ . This mode bears strong resemblance to one of the interaction sensitive modes for the case of two distinguishable particles discussed in the beginning of this section. Its frequency is mainly affected by  $g_{AB}$  and barely by  $g_{\sigma}$ . The detection of this breathing frequency requires a numerical approach capable to incorporate the entanglement between the components (beyond species mean-field) and a preparation scheme which initializes a state having a sizable overlap with the corresponding eigenstate of odd CM parity.

### B. Bose polaron

Now we turn our attention to a single impurity  $N_B = 1$  in a few-body majority environment having  $N_A = 5$  or  $N_A = 10$  particles. In contrast to [65], here, we relax only the  $B$  component, while the  $A$  component is affected indirectly via the inter-component coupling  $g_{AB}$ . At  $\eta = 1$  the CM motion still decouples from the relative motions. In particular, the quench operator may mediate between eigenstates of different CM parity inducing eventually a special breathing mode caused by population of an eigenstate with odd CM parity. Furthermore, there is only one particle in the  $B$  component. Thus, a double excitation state  $|N_A\rangle \otimes |N_B - 2, 2\rangle$  (see Section IV A) does not exist and we expect that one of the relative modes (black curves in Fig. 3), whose frequency is notably affected by interactions, will not be present.

In Figs. 4 and 5 we show the excitation spectrum of the breathing dynamics initialized by quenching the equilibrated system at trap ratio  $\eta = 1.05$  to  $\eta = 1$ , i.e., partially releasing the trap of the impurity. The majority component consists of  $N_A = 5$  (Fig. 4) or  $N_A = 10$  (Fig. 5) particles subject to several different majority component interactions  $g_A$  (subfigures a-c). Only frequencies of modes whose contribution is above 10% of the maximum amplitude  $\Sigma_{\max}$  in the averaged power spectrum are shown. Additionally, each frequency data point

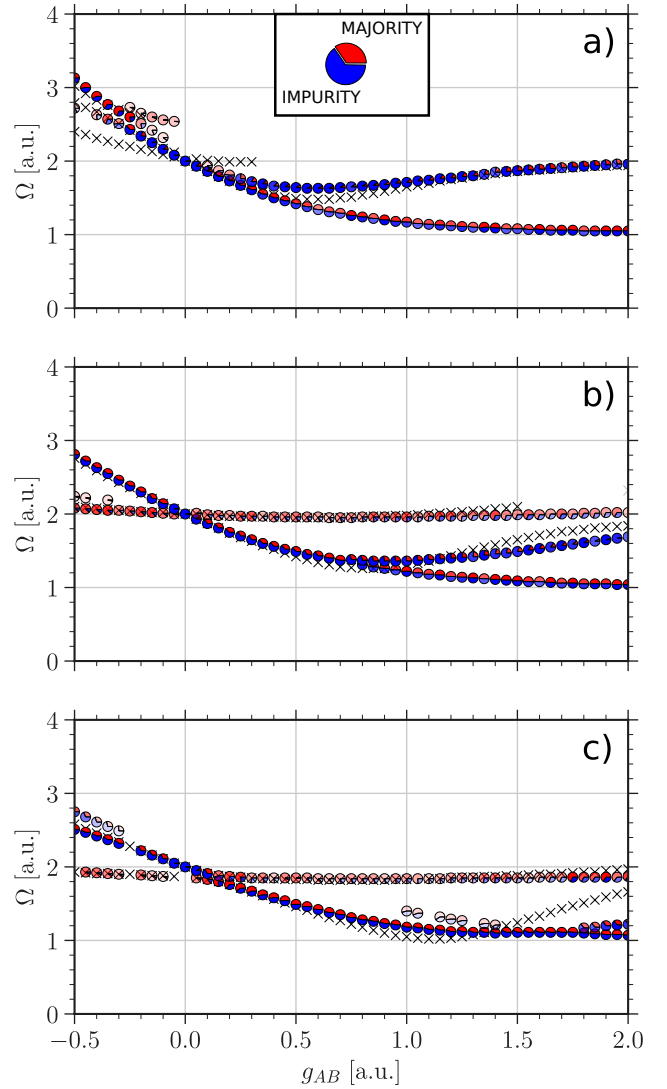


Figure 4. Frequencies  $\Omega$  of breathing modes excited by quenching the ground state  $|E_0\rangle$  of the Bose polaron for  $N_A = 5$  and  $N_B = 1$ , meaning a change in the trap ratio from  $\eta = 1.05$  to  $\eta = 1.0$ , shown as a function of the inter-component coupling  $g_{AB}$  for a fixed majority component interaction a)  $g_A = -0.5$ , b)  $g_A = 0$  and c)  $g_A = 0.5$ . Each frequency data point (full circle) is divided into two sectors of different colors representing the contribution of the breathing observables  $\langle \sum_i \hat{x}_i^2 \rangle_t$  (red) or  $\langle \hat{y}^2 \rangle_t$  (blue) to the averaged power spectrum  $\Sigma$  at that frequency (see Section III B). The corresponding color intensity indicates the relative strength w.r.t. the maximum amplitude  $\Sigma_{\max}$  in the averaged power spectrum for fixed  $g_{AB}$  and only modes with contribution above 10% of  $\Sigma_{\max}$  are presented. Crosses stand for frequencies of modes excited within the SMF approximation.

(full circle) is represented as a pie chart of two different colors and encodes the contribution of the breathing observables to the averaged power spectrum (see Section III B): blue color for the impurity  $\hat{y}^2$  and red color for the majority component  $\sum_i \hat{x}_i^2$ . The decomposition

<sup>2</sup> corresponding to a map  $x_i \mapsto y_i$  at  $g_A = g_B$

into colors tells us whether the respective mode is a single species mode or whether it is of a mixed character and to what extent. Furthermore, the color intensity indicates the participation of the respective mode in the breathing dynamics as compared to the most relevant mode at fixed  $g_{AB}$  (a more intense color indicates a stronger contribution). Finally, the crosses represent frequencies of modes excited by the same procedure but numerically ignoring the entanglement in the initial state and the subsequent dynamics (SMF approximation).

Let us first focus on Fig. 4b, the case of a non-interacting majority species ( $g_A = 0$ ). At  $g_{AB} = 0$  only the impurity is excited (blue circle) performing a breathing motion with frequency  $\Omega = 2$  as expected. As one increases the coupling strength ( $g_{AB} > 0$ ), a second mode of decreasing frequency emerges resulting in a beating. This mode has the largest contribution to the ongoing dynamics and is more prominent in the impurity motion. The frequency of the other mode experiences only a slight variation  $\Omega \approx 2$  and is represented to a larger extent in the majority component. It matches the behavior of the relative mode least sensitive to interactions encountered in Section IV A (cf. black curves in Fig. 3).

Around  $g_{AB} \approx 0.75$  the lower frequency splits into two branches of comparable significance resulting altogether in three modes. One of the emerging branches possesses a continuously decreasing frequency with increasing  $g_{AB}$  approaching the value  $\Omega = 1$ . It matches the description of the inter-component mode which is caused by an eigenstate of odd CM parity and was emphasized in Section IV A (cf. red curve in Fig. 3). Interestingly, it is equally represented in both subsystems despite the particle number imbalance and quench asymmetry. The other frequency branch bends and starts recovering towards  $\Omega = 2$  with increasing  $g_{AB}$  while gradually becoming a pure signature of the impurity motion only (the blue slice dominates at  $g_{AB} = 2$ ). It reminds of the two convex mode frequencies particularly sensitive to interactions mentioned in Section IV A (cf. the black curves in Fig. 3).

At weak negative coupling ( $g_{AB} < 0$ ) one observes also a beating behavior, although here both frequencies are increasing with decreasing  $g_{AB}$ . The dominant frequency in the power spectrum is more sensitive to the coupling variation and dominates the impurity motion, while the second is barely affected and primarily represented in the majority component. Below a certain threshold ( $g_{AB} < -0.4$ ) one observes low-amplitude traces of a third frequency.

We discover several major alternations in the excitation spectrum when the majority component becomes interacting. For weakly attractive ( $g_A = -0.5$ ) majority particles in Fig. 4a the coupling-insensitive mode frequency is seemingly absent. At positive increasing  $g_{AB}$  the bifurcation of the continuously decaying frequency takes place already for a very weak coupling strength ( $g_{AB} \approx 0.1$ ). The character of the excited modes is mostly the same as for  $g_A = 0$ . At negative decreasing

$g_{AB}$  we observe an emerging multi-frequency breathing composed of three modes. The lower-frequency mode loses amplitude in favor of higher-frequency modes ( $-0.4 < g_{AB} < -0.1$ ). Then it turns into a single-frequency breathing ( $g_{AB} < -0.4$ ) affecting both components in a similar way.

For weakly repulsive ( $g_A = 0.5$ ) majority particles in Fig. 4c the coupling-insensitive mode frequency is still present though energetically shifted downwards to  $\Omega = 1.9$ . The respective mode is weakly represented in the overall dynamics and affects mainly the majority component. The point of bifurcation in the lower frequency branch is located at a stronger coupling  $g_{AB} \approx 1.8$ . At negative  $g_{AB}$  below a certain threshold ( $g_{AB} < -0.3$ ) a third mode is excited. In contrast to  $g_A = 0$ , this additional mode is rather manifested in the impurity breathing and has a larger frequency. In summary, the majority component interaction  $g_A$  determines the coupling value at which the bifurcation takes place as well as the offset of the coupling-insensitive frequency and whether it can be addressed by the current quench protocol.

Next, we double the number of majority component atoms to get an idea of how it affects the excitation spectrum. In the following, we compare the corresponding subfigures of Figs. 4 and 5. We note that at  $N_A = 10$  the interval of the considered couplings is  $g_{AB} \in [-0.5, 1.0]$  as the convergence is more challenging to achieve beyond  $g_{AB} > 1$ . At  $g_A = 0$  (Fig. 5b) the bifurcation point is located at a smaller value of  $g_{AB}$  compared to the  $N_A = 5$  case (see Fig. 4b). After the bifurcation, we observe a decreasing relevance of the lower frequency mode in favor of the upper branch. We anticipate that its amplitude will decay further for an even larger number of majority atoms. The coupling-insensitive mode frequency is barely affected by the particle number imbalance.

At  $g_A = -0.5$  (Fig. 5a) and positive  $g_{AB}$  the minimum of the convex frequency mode is shifted to larger frequencies and smaller values of the coupling  $g_{AB}$ . The frequency value recovers back to  $\Omega = 2$  more quickly already at  $g_{AB} \approx 0.75$ . The coupling-insensitive mode becomes visible at negative  $g_{AB}$  and even dominates the breathing dynamics, although the amplitude decays considerably towards  $g_{AB} = 0$  and there are only minor traces left at positive coupling ( $0.25 < g_{AB} < 0.4$ ). It is certainly present in the breathing dynamics at positive  $g_{AB}$ , but the contribution is not significant enough to overcome the set threshold. The respective frequency is shifted to  $\Omega \approx 2.4$ . At  $g_A = 0.5$  (Fig. 5c) the frequency of the coupling-insensitive mode experiences a slight shift downwards. At negative  $g_{AB}$  it gains amplitude with decreasing  $g_{AB}$  until it becomes a dominant mode below  $g_{AB} \leq -0.25$ . The bifurcation point at positive  $g_{AB}$  is unfortunately not visible within the covered  $g_{AB}$  interval.

Lastly, we want to address the importance of entanglement in our Bose polaron setup. To this end we neglect it both in the initial state and in the subsequent dynamics (crosses in Figs. 4 and 5). The first striking observation is that in this case at most *two* frequencies can



be extracted. The mode we are missing from the exact simulations is the one whose frequency is a monotonically decreasing function of  $g_{AB}$ . Regarding the persistent modes, the one with a coupling-insensitive frequency is overall well-captured by the species mean-field ansatz, although it tends to overestimate the frequency for large positive values of  $g_{AB}$ . The other one, whose frequency is a convex function of  $g_{AB}$ , in general fails to match the corresponding exact frequency: either mispredicting the location (Fig. 4c) or the exact value (Fig. 4a) of the minimum. Even if both the location and the value of the minimum are well-matched (Fig. 4b) there is an increasing discrepancy for strong positive  $g_{AB}$ . For a larger particle number (Fig. 5) the consistency between approximated and exact frequencies is much better, though also here one mode is missing.

To summarize, we are able to excite up to three breathing modes in the Bose polaron setup by quenching only the impurity. First, there is a coupling-insensitive mode frequency whose value can be manipulated by the particle number imbalance or the majority component interaction. Second, there is a monotonically decreasing frequency converging towards  $\Omega = 1.0$  with increasing  $g_{AB}$ . It cannot be described by the species mean-field ansatz and its contribution to the ongoing dynamics decreases with larger particle number imbalance. Third, at a sufficiently strong coupling an additional mode enters the dynamics. The mode frequency is a convex function of  $g_{AB}$  with a minimum being sensitive to  $g_A$  and  $N_A$ .

### C. Impact of the trap

Let us now focus on the impact of the external trap, more specifically we consider a situation where the length scale of the impurity  $l_B = \sqrt{1/\eta}$ , set by the parabolic trap, is either broader ( $l_B = 1.4$ ) or narrower ( $l_B = 0.5$ ) in the post-quench system. The quench strength is still 5% of the original trap parameter.

We start with the case of a 'broad' impurity  $N_B = 1$ . In Fig. 6a and Fig. 7a we show the breathing spectrum for  $N_A = 5$  and  $N_A = 10$  majority atoms, respectively. To gain an intuitive picture we set  $g_A = 0$ . For the decoupled case  $g_{AB} = 0$ , the lowest frequency mode is caused by the eigenstate  $|N_A\rangle \otimes |0, 0, 1\rangle$ , corresponding to a standard breathing of the impurity at frequency  $\Omega = 1.02$ . It is the only mode excited. Once coupled ( $g_{AB} \neq 0$ ), several other eigenstates may become populated leading to additional breathing modes. The states in question can be continuously traced back to the low-energy eigenstates of a decoupled impurity. First, we have the state  $|N_A - 1, 1\rangle \otimes |0, 1\rangle$  corresponding to an excitation of a sloshing mode in each component at frequency  $\Omega = 1.51$ . Then follows a quasi-degenerate manifold of three modes: two majority component modes at the same frequency  $\Omega = 2$  caused by  $|N_A - 1, 0, 1\rangle \otimes |1\rangle$  and  $|N_A - 2, 2\rangle \otimes |1\rangle$ , and a second order breathing of the impurity at frequency  $\Omega = 2.04$  mediated by  $|N_A\rangle \otimes |0, 0, 0, 1\rangle$ . Any higher

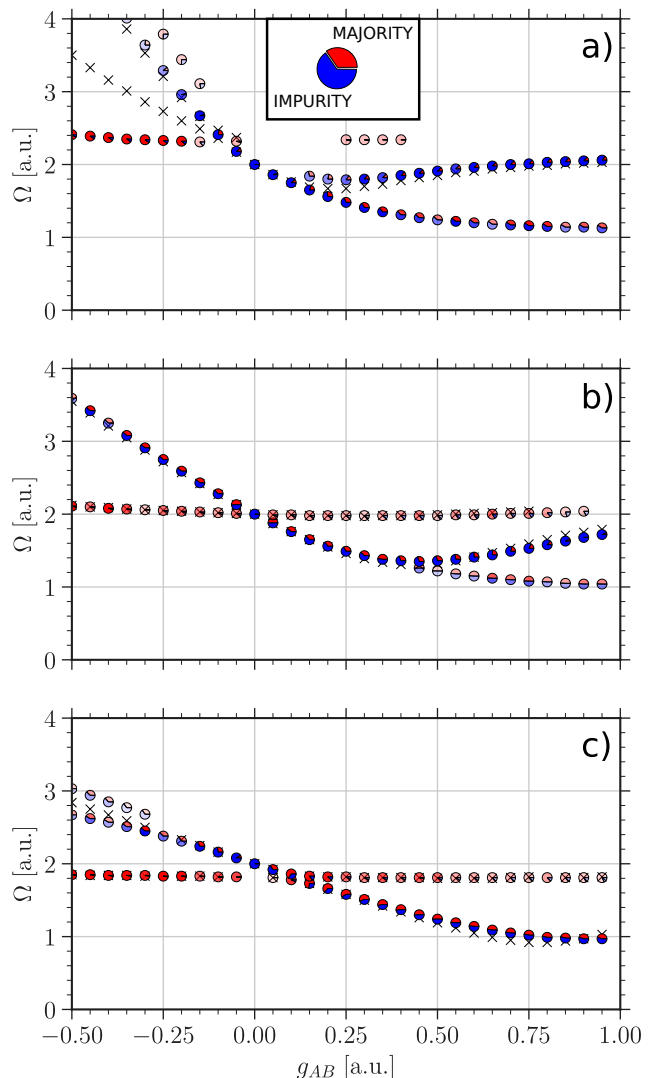


Figure 5. Same as in Fig. 4 but for  $N_A = 10$ .

frequency modes are unlikely to be involved.

At weak coupling  $g_{AB}$  there is only one relevant mode excited. It originates from the state  $|N_A\rangle \otimes |0, 0, 1\rangle$  and is barely detectable in the majority component breathing. The corresponding frequency is a convex function of  $g_{AB}$  with a minimum at  $g_{AB} \approx 0.5$  for  $N_A = 5$  (Fig. 6a) and at  $g_{AB} \approx 0.25$  for  $N_A = 10$  (Fig. 7a). At strong positive  $g_{AB}$  a beating behavior emerges. The amplitude of the additional mode increases gradually with increasing  $g_{AB}$  while the corresponding frequency  $\Omega \approx 1.2$  is only weakly affected by the inter-component coupling or the particle number. At negative moderate  $g_{AB}$  there is also a beating. The major amplitude mode, originally being an impurity mode (blue), evolves gradually into the majority component mode (red). The other mode appears just below  $g_{AB} < -0.25$  and affects primarily the majority species.

The SMF fits well the lowest frequency at negative  $g_{AB}$

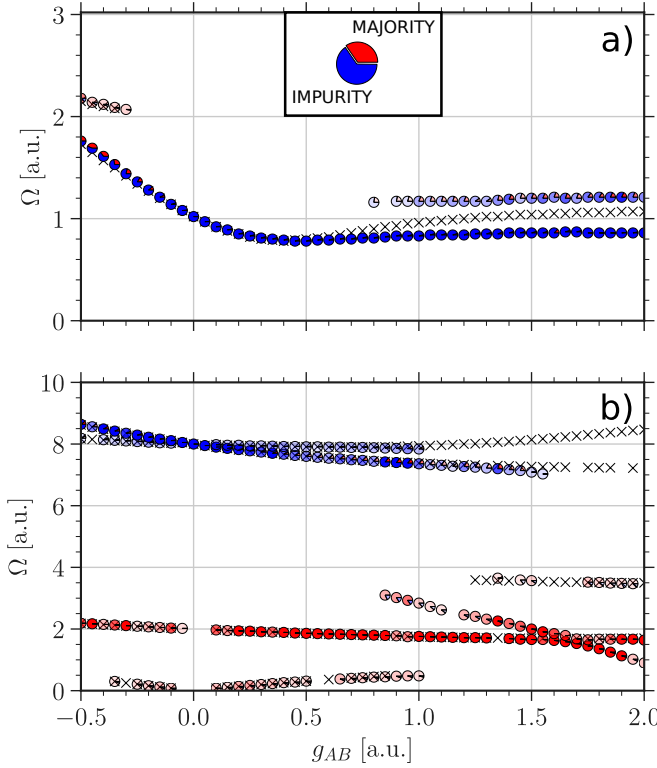


Figure 6. Frequencies  $\Omega$  of breathing modes for  $N_A = 5$  and  $N_B = 1$  as a function of the inter-component coupling  $g_{AB}$  at fixed majority component interaction  $g_A = 0$ . The trap ratio is quenched in (a) from  $\eta = 0.536$  to  $\eta = 0.51$  and in (b) from  $\eta = 4.2$  to  $\eta = 4$ . Color coding according to Fig. 4.

and at weak positive  $g_{AB}$  until the minimum is reached. Afterwards, it overestimates the frequency having larger deviations at stronger positive  $g_{AB}$ . Again, we witness that SMF is incapable to identify an emerging mode at positive  $g_{AB}$ , though at negative  $g_{AB}$  it does register the beating behavior. It implies that the additional modes entering the dynamics at positive and negative  $g_{AB}$  are of a different character. Based on the insights gained in the previous section, namely the presence of a breathing mode which is inaccessible to the SMF treatment, we conjecture that the higher frequency mode observed at positive  $g_{AB}$  stems from the doubly excited sloshing mode  $|N_A - 1, 1\rangle \otimes |0, 1\rangle$  at  $g_{AB} = 0$ . Its contribution grows as the entanglement becomes stronger.

Next, let us focus on the case of a ‘narrow’ impurity  $N_B = 1$ . The corresponding breathing spectrum is depicted in Fig. 6b for  $N_A = 5$  and in Fig. 7b for  $N_A = 10$  majority atoms. At  $g_{AB} = 0$  we excite only the standard breathing mode of the impurity at frequency  $\Omega = 8$  caused by the eigenstate  $|N_A\rangle \otimes |0, 0, 1\rangle$ . Considering the amount of available even parity eigenstates with energies up to eight quanta (40 for  $N_A = 5$  and 45 for  $N_A = 10$ ), one might naively think that many modes would be excited at finite  $g_{AB}$ . This is not the case as we count only up to six frequencies. They are well separated from

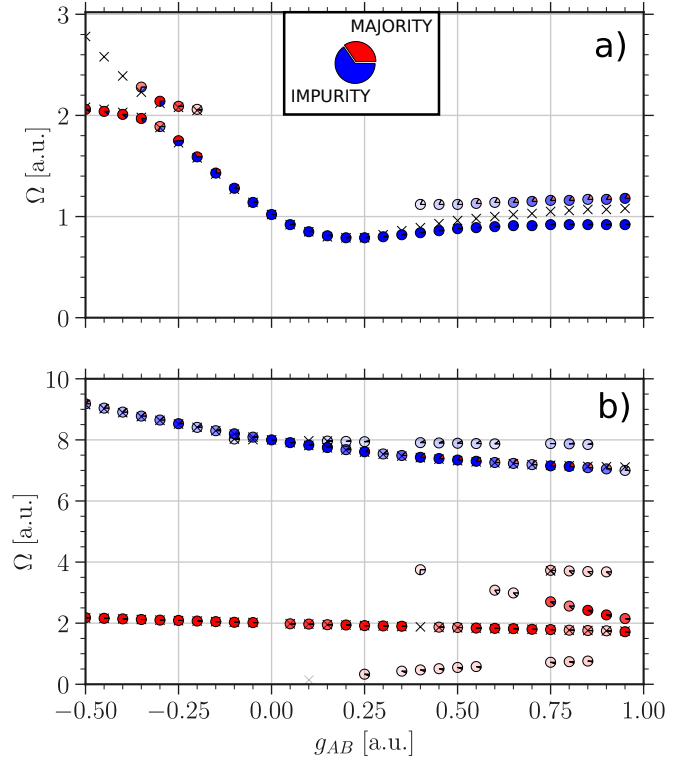


Figure 7. Same as in Fig. 6 but for  $N_A = 10$ .

each other and admit a convenient classification: impurity modes (blue) with  $\Omega > 6$  and majority modes (red) with  $\Omega < 4$ .

The impurity features a beating composed of two modes at weak coupling. The gap between the corresponding frequencies grows with increasing  $g_{AB}$ . The one of smaller amplitude vanishes around  $g_{AB} \approx 1.0$ . The contribution of the other mode fades away quickly afterwards until it also disappears. At strong  $g_{AB}$  the impurity motion assimilates the majority component breathing. Both modes are reproducible by SMF ansatz, though SMF overestimates their contribution to the overall dynamics at strong  $g_{AB}$ .

Regarding the majority modes there is one with a nearly constant frequency ( $\Omega \approx 2$ ) entering the dynamics already at weak coupling and making a large contribution to the majority motion across all coupling values. At weak  $g_{AB}$  it is accompanied by an oscillation of a smaller frequency. As the ground state is non-degenerate at  $g_{AB} = 0$ , this frequency corresponds to the gap between the two blue-colored frequencies. It also consistently disappears beyond  $g_{AB} > 1$  along with the impurity modes. The latter are actually replaced by modes of lower frequency. One of them is of particular interest. It appears at  $g_{AB} \approx 1$  for  $N_A = 5$  and at  $g_{AB} \approx 0.5$  for  $N_A = 10$  gaining weight with increasing  $g_{AB}$ . The corresponding frequency is a linearly decreasing function of  $g_{AB}$ . It can be interpolated to frequency  $\Omega = 5$  at  $g_{AB} = 0$ , matching the energy gap between the ground

state  $|N_A\rangle \otimes |1\rangle$  and the inter-component sloshing mode eigenstate  $|N_A - 1, 1\rangle \otimes |0, 1\rangle$ . The entanglement is once again indispensable to account for the respective breathing mode.

#### D. Breathing of the first excited state

The Hamiltonian Eq. (1) has global reflection symmetry. The eigenstates are therefore separable into two classes of even and odd global parity. The quench operator does not violate that symmetry. Accordingly, an even parity initial state can be expanded within the subspace of even eigenstates. The odd parity space of the Hamiltonian has its own 'ground state', meaning the lowest energy eigenstate of that subspace. If initialized in such a state, how will each species respond following our quench procedure? Will it be a few-mode breathing within each component, as for the even parity ground state, or a more complex motion involving many modes? If only a few modes participate, how different are the respective frequencies as compared to the even parity ground state?

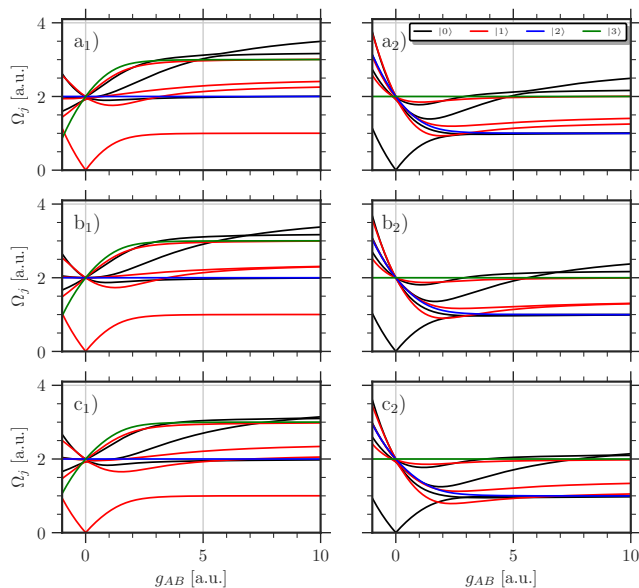


Figure 8. Energy gaps  $\Omega_j = |E_j - E_{\text{ref}}|$  w.r.t. lowest energy reference eigenstates  $|E_{\text{ref}}\rangle$  of odd global parity and even (first column) or odd (second column) CM parity in a few-body bosonic mixture  $N_A = N_B = 2$ . The gaps are functions of the inter-component coupling  $g_{AB}$  at equal trapping frequency ratio  $\eta = 1$ , intra-component interaction strength  $g_A = 0$  for the first component and a)  $g_B = -0.5$ , b)  $g_B = 0$ , c)  $g_B = 0.5$  for the second component. Whether the modes are actually excited depends on the quench protocol. Different colors refer to the center-of-mass (CM) quantum number in the eigenstate  $|E_j\rangle$ . The CM is a decoupled degree of freedom in this harmonic confinement.

To address the above questions, we consider again the example of a particle-balanced few-body Bose mixture

(see Section IV A) at  $\eta = 1$ . We notice that in the non-interacting regime the odd parity 'ground state' is two-fold degenerate, composed of states where a single particle of either component is excited by one energy quantum:  $|N_A - 1, 1\rangle \otimes |N_B\rangle$  and  $|N_A\rangle \otimes |N_B - 1, 1\rangle$  w.r.t. harmonic oscillator basis. Once the degeneracy is lifted at finite coupling the perturbed eigenstates can be distinguished by the CM quantum number. As both of them are likely to be populated after the quench, we account for both as reference states when evaluating the energy gaps to neighboring eigenstates. The frequencies of breathing oscillations following a quench of the impurity trap will be contained within the set of these energy gaps. At zero interactions, the energetically closest potentially accessible neighboring eigenstates are the three quanta excitations. There are eight of them in total. Half of them are excitations within a single component:  $|N_A - 1, 0, 0, 1\rangle$ ,  $|N_A - 2, 1, 1\rangle$  and the same for  $B$  species. The other four distribute the three available quanta over both components:  $|N_A - 1, 1\rangle \otimes |N_B - 2, 2\rangle$ ,  $|N_A - 1, 0, 1\rangle \otimes |N_B - 1, 1\rangle$  and the other way around ( $B \leftrightarrow A$ ).

In Fig. 8 we show the energy gaps between a reference state of even or odd CM parity (first or second column respectively) and energetically closest eigenstates (CM quantum number indicated by color) as a function of the inter-component coupling  $g_{AB}$  for three different intra-component interaction regimes (rows).

Let us begin with the reference state of even CM parity (first column). First, there is a single constant frequency mode  $\Omega = 2$  (blue) for any interaction values. Second, there is a single frequency being a monotonically increasing function of  $g_{AB}$  (green) and saturating to  $\Omega = 3$  at strong positive  $g_{AB}$ . Third, among the three black curves there is one very weakly dependent on the interactions and it recovers to  $\Omega = 2$  at strong positive  $g_{AB}$ , whereas the other two are highly susceptible to interactions and reach values beyond  $\Omega = 3$ . Finally, the lower red curve represents the other reference state of odd CM parity. Regarding the frequencies of the remaining three red modes, one of them behaves similar to the green mode, while the other two are highly sensitive to interactions. Some of the crossings seen at  $g_B = 0$  (subfigure b) among the black and red curves become avoided at finite  $g_B$  (subfigures a and c) caused by broken species exchange symmetry. Overall, most frequencies reach values above  $\Omega = 2$  and there is nothing common to the breathing spectrum of the even CM-parity ground state (see Fig. 3) except the constant frequency mode.

Focusing now on the reference state of odd CM-parity (second column), we notice that all five frequencies encountered in Fig. 3 have here a corresponding match. The reason is that the reference state is a simple CM excitation, being a constant energy shift independent of the interaction strength. Correspondingly, the even parity ground state and the eigenstates responsible for the first order breathing modes discussed in Section IV A are just spectrally shifted by a common constant. Thus, the

corresponding energy gaps remain intact. The four black curves are the additional new modes. The lowest one corresponds to the even CM-parity reference state of odd global parity. There is one with a monotonically decreasing frequency and two of them are convex functions of  $g_{AB}$  very sensitive to interactions akin to the red mode frequencies.

In the Bose polaron setup there are two less 'three-quanta' states, since the two-particle excitations of the impurity are obviously excluded. However, there is also one more state, namely a three-particle excitation  $|N_B - 3, 3\rangle$  in the majority component. Thus, there are seven addressable low-energy eigenstates in total. Now, we initialize an odd parity 'ground state' for the subsequent breathing dynamics and extract the frequencies of participating modes shown in Fig. 9. We immediately recognize the frequency pattern from Fig. 4. In particular, we evidence a coupling-insensitive frequency at  $\Omega \approx 2$ , a monotonically decaying one converging to  $\Omega = 1$  and one which is a convex function of  $g_{AB}$ . There are however several differences. Importantly, both odd parity 'ground states' are participating in the dynamics, as indicated by the lowest frequency curve. The excitation pattern implies that the odd-CM 'ground state' has a larger contribution than the one of even-CM. Second, at weak positive  $g_{AB}$  the two odd parity reference states are dominating the dynamics. The energy gap between them grows with increasing  $g_{AB}$  and approaches its limiting value  $\Omega = 1$ . Meanwhile, there is a gradual transfer of population to the eigenstate responsible for the breathing frequency which is monotonically decaying function of  $g_{AB}$ . Finally, at  $g_A = 0.5$  and positive intermediate  $g_{AB} \approx 1$  as well as at negative  $g_{AB}$  we identify some minor traces of additional modes absent for the even parity ground state.

## V. SUMMARY AND CONCLUSIONS

The breathing dynamics of a few-body Bose polaron in a one-dimensional species-selective parabolic confinement has been investigated in this work by means of the Multi-Layer Multi-Configuration Time-Dependent Hartree Method for Bosons. The dynamics has been triggered by a weak trap quench of the impurity for different inter-component couplings  $g_{AB}$  ranging from weak attractive to intermediate repulsive values. The majority motion was affected indirectly via the majority-impurity interaction  $g_{AB}$ . We extracted the frequencies of excited modes from the breathing observables by using a Compressed Sensing algorithm. From this we constructed an averaged power spectrum and classified the modes according to their overall contribution to the dynamics. We also determined whether a mode is of majority or impurity type judged by the relative strength of respective observables in the averaged power spectrum. To highlight the importance of entanglement in our setup we performed the same quench procedure for a species-mean

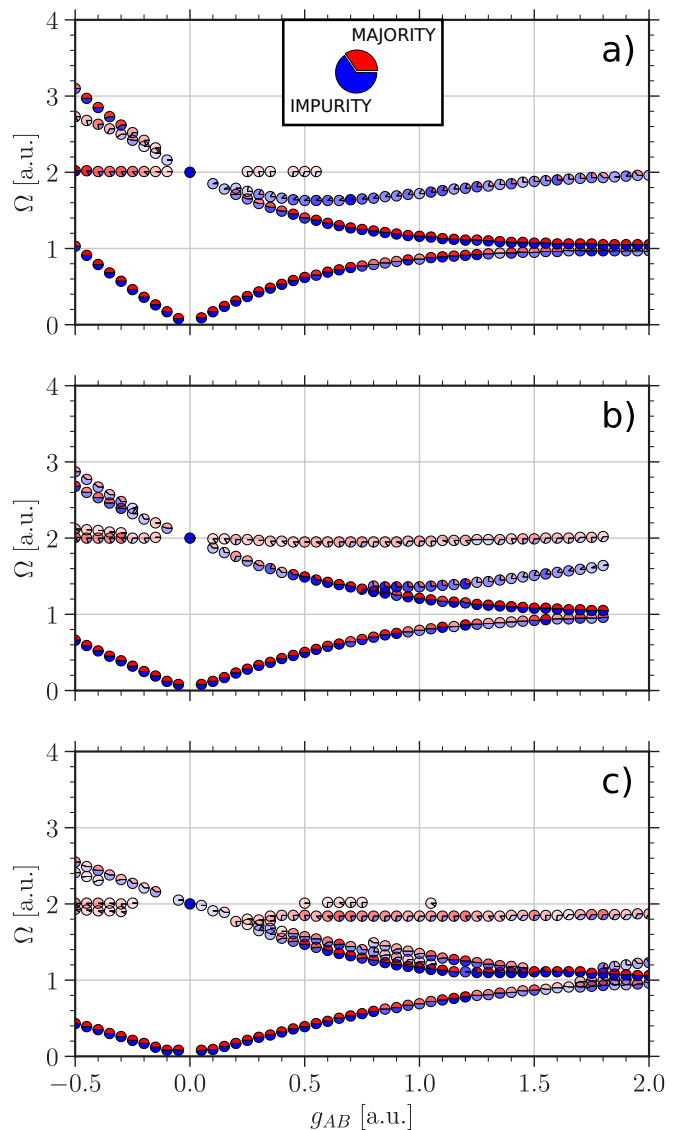


Figure 9. Frequencies  $\Omega$  of breathing modes excited by quenching the odd parity 'ground state'  $|E_1\rangle$  of a Bose polaron  $N_A = 5$  and  $N_B = 1$  from a trap ratio  $\eta = 1.05$  to  $\eta = 1.0$  as a function of the inter-component coupling  $g_{AB}$  for a fixed majority component interaction a)  $g_A = -0.5$ , b)  $g_A = 0$  and c)  $g_A = 0.5$ . Color coding as in Fig. 4.

field ansatz, which assumes that a wave-function can be written as a single product state of combined majority coordinates and the impurity coordinate.

Different regimes of system parameters have been addressed. The majority component was non-interacting ( $g_A = 0$ ), weakly attractive ( $g_A = -0.5$ ) or weakly repulsive ( $g_A = 0.5$ ) consisting either of  $N_A = 5$  or  $N_A = 10$  particles and different ratios of species trapping frequencies including equal localization length ( $\eta = 1$ ), a 'broad' impurity ( $\eta = 0.51$ ) and a 'narrow' impurity ( $\eta = 4.0$ ) have been taken into account. Finally, we studied the impact of parity symmetry on the breathing spectrum.

To this end, we initialized the system in the first excited state having odd global parity as opposed to the ground state which is even.

For equal traps ( $\eta = 1$ ) we detected up to three modes. First, at a weak majority-impurity interaction there is a beating. One mode is of a majority type. It does a comparatively small contribution to the overall breathing dynamics while its frequency is insensitive to  $g_{AB}$  variations, albeit depending on  $g_A$  and  $N_A$ . The mode becomes suppressed for a weakly attractive majority species at positive  $g_{AB}$ . The frequency of the second mode decreases monotonically as a function of  $g_{AB}$  until it bifurcates into two distinct frequencies. One of them keeps decreasing. Other parameters such as majority-component interaction strength  $g_A$  or the number of majority atoms  $N_A$  barely affect this frequency. The corresponding mode is caused by an eigenstate of odd CM parity and even global parity. The mode is equally represented in both components while its existence depends on the entanglement. The other emerging frequency bends evolving into a convex function of the majority-impurity interaction. The position of the minimum is very sensitive to  $g_A$  and  $N_A$ . The mode dominates the impurity motion.

By broadening the impurity trap ( $\eta = 0.51$ ) only one mode can be excited at weak  $g_{AB}$ . It is of impurity type while the corresponding frequency behaves as a convex function of  $g_{AB}$ . With increasing impurity-majority interaction a beating emerges. At positive  $g_{AB}$  the additional mode is caused by the entanglement, while at negative  $g_{AB}$  both frequencies are well-matched by the SMF ansatz. For a tightly trapped impurity ( $\eta = 4$ ) up to six frequencies can be observed, though many more modes are in principle available. The two impurity type modes are of high frequency but are quickly fading away with increasing  $g_{AB}$ . At strong  $g_{AB}$  the impurity oscillations start imitating the majority motion. Among the lower frequency majority type modes there is one of major amplitude across all  $g_{AB}$ . The corresponding frequency is coupling-insensitive. Among the modes emerging at finite  $g_{AB}$  we emphasized the one caused by the entanglement.

With increasing  $g_{AB}$  the mode amplitude is enhanced while its frequency quickly decays.

Regarding the first excited state of odd global parity as an initial state for the breathing dynamics, we found the corresponding excitation spectrum to bear strong similarity to the one of even parity ground state. It can be understood as follows. Some of eigenstates lying in the odd parity subspace have energies corresponding to the ones of even parity subspace except for a constant energy shift, which is an integer number (in harmonic units) corresponding to a center-of-mass excitation. Nevertheless, there are also differences. There is a slow-frequency mode equally represented in both components. It is caused by the degeneracy of the first excited state. The frequency starts at  $\Omega = 0$  and saturates towards  $\Omega = 1$  with increasing  $g_{AB}$ . For a weakly repulsive majority species and at intermediate  $g_{AB}$  we also observe several additional modes absent in the ground state spectrum.

Overall, the few-body Bose-polaron breathing spectrum has been studied and compared to the one of a particle-balanced Bose-Bose mixture. The quench protocol employed in this work allowed to couple eigenstates of different CM parity (at  $\eta = 1$ ) as opposed to a species-symmetric trap quench. We excited a new kind of a breathing mode. The eigenstate responsible for this mode has odd CM parity ( $\eta = 1$ ) or can be traced back to an inter-component sloshing excitation at zero interactions ( $\eta \neq 1$ ). The mode relies on the presence of entanglement, while its frequency is a monotonically decreasing function of  $g_{AB}$ . This opens the perspective to study the relation between the mode amplitude and the degree of entanglement, stored in the many-body composite state, adding yet another item into the analysis toolbox of breathing mode diagnostics.

## ACKNOWLEDGMENTS

M. P. gratefully acknowledges a scholarship of the Studienstiftung des deutschen Volkes.

- 
- [1] L. D. Landau, Phys. Z. **3**, 664 (1933).
  - [2] S. Pekar, Sov. Phys. JETP **16**, 341 (1946).
  - [3] J. T. Devreese and A. S. Alexandrov, Rep. Prog. Phys. **72**, 066501 (2009).
  - [4] A. S. Alexandrov and J. T. Devreese, *Advances in polaron physics*, Vol. 159 (Springer, 2010).
  - [5] G. D. Mahan, *Many-particle physics* (Springer Science & Business Media, 2013).
  - [6] M. H. Anderson, J. R. Ensher, M. R. Matthews, C. E. Wieman, and E. A. Cornell, Science **269**, 198 (1995).
  - [7] K. B. Davis, M.-O. Mewes, M. R. Andrews, N. J. van Druten, D. S. Durfee, D. Kurn, and W. Ketterle, Phys. Rev. Lett. **75**, 3969 (1995).
  - [8] I. Bloch, J. Dalibard, and W. Zwerger, Rev. Mod. Phys. **80**, 885 (2008).
  - [9] C. Myatt, E. Burt, R. Ghrist, E. A. Cornell, and C. Wieman, Phys. Rev. Lett. **78**, 586 (1997).
  - [10] D. Blume, Rep. Prog. Phys. **75**, 046401 (2012).
  - [11] S. Palzer, C. Zipkes, C. Sias, and M. Köhl, Phys. Rev. Lett. **103**, 150601 (2009).
  - [12] J. Catani, G. Lamporesi, D. Naik, M. Gring, M. Inguscio, F. Minardi, A. Kantian, and T. Giamarchi, Phys. Rev. A **85**, 023623 (2012).
  - [13] T. Fukuhara, A. Kantian, M. Endres, M. Cheneau, P. Schauß, S. Hild, D. Bellem, U. Schollwöck, T. Giamarchi, C. Gross, *et al.*, Nat. Phys. **9**, 235 (2013).
  - [14] N. Spethmann, F. Kindermann, S. John, C. Weber, D. Meschede, and A. Widera, Phys. Rev. Lett. **109**, 235301 (2012).
  - [15] N. B. Jørgensen, L. Wacker, K. T. Skalmstang, M. M. Parish, J. Levinsen, R. S. Christensen, G. M. Bruun, and J. J. Arlt, Phys. Rev. Lett. **117**, 055302 (2016).

- [16] F. Meinert, M. Knap, E. Kirilov, K. Jag-Lauber, M. B. Zvonarev, E. Demler, and H.-C. Nägerl, *Science* **356**, 945 (2017).
- [17] S. Nascimbene, N. Navon, K. Jiang, L. Tarruell, M. Teichmann, J. McKeever, F. Chevy, and C. Salomon, *Phys. Rev. Lett.* **103**, 170402 (2009).
- [18] A. Schirotzek, C.-H. Wu, A. Sommer, and M. W. Zwierlein, *Phys. Rev. Lett.* **102**, 230402 (2009).
- [19] M. Koschorreck, D. Pertot, E. Vogt, B. Fröhlich, M. Feld, and M. Köhl, *Nature* **485**, 619 (2012).
- [20] C. Kohstall, M. Zaccanti, M. Jag, A. Trenkwalder, P. Massignan, G. M. Bruun, F. Schreck, and R. Grimm, *Nature* **485**, 615 (2012).
- [21] M. Cetina, M. Jag, R. S. Lous, J. T. Walraven, R. Grimm, R. S. Christensen, and G. M. Bruun, *Phys. Rev. Lett.* **115**, 135302 (2015).
- [22] F. Grusdt and E. Demler, *Quantum Matter at Ultralow Temperatures* **191**, 325 (2015).
- [23] F. Chevy and C. Mora, *Rep. Prog. Phys.* **73**, 112401 (2010).
- [24] P. Massignan, M. Zaccanti, and G. M. Bruun, *Rep. Prog. Phys.* **77**, 034401 (2014).
- [25] H. Fröhlich, *Adv. Phys.* **3**, 325 (1954).
- [26] C. Chin, R. Grimm, P. Julienne, and E. Tiesinga, *Rev. Mod. Phys.* **82**, 1225 (2010).
- [27] T. Köhler, K. Góral, and P. S. Julienne, *Rev. Mod. Phys.* **78**, 1311 (2006).
- [28] A. Volosniev and H.-W. Hammer, *Phys. Rev. A* **96**, 031601 (2017).
- [29] F. Grusdt, G. E. Astrakharchik, and E. Demler, *New J. Phys.* **19**, 103035 (2017).
- [30] F. Grusdt, K. Seetharam, Y. Shchadilova, and E. Demler, *Phys. Rev. A* **97**, 033612 (2018).
- [31] B. Kain and H. Y. Ling, *Phys. Rev. A* **98**, 033610 (2018).
- [32] M. Drescher, M. Salmhofer, and T. Enss, *Phys. Rev. A* **99**, 023601 (2019).
- [33] J. Jager, R. Barnett, M. Will, and M. Fleischhauer, *Phys. Rev. Res.* **2**, 033142 (2020).
- [34] M. Drescher, M. Salmhofer, and T. Enss, *Phys. Rev. Res.* **2**, 032011 (2020).
- [35] T. Giamarchi, *Quantum physics in one dimension*, Vol. 121 (Clarendon press, 2003).
- [36] M. Olshanii, *Phys. Rev. Lett.* **81**, 938 (1998).
- [37] T. Bergeman, M. Moore, and M. Olshanii, *Phys. Rev. Lett.* **91**, 163201 (2003).
- [38] E. Haller, M. J. Mark, R. Hart, J. G. Danzl, L. Reichsöllner, V. Melezhik, P. Schmelcher, and H.-C. Nägerl, *Phys. Rev. Lett.* **104**, 153203 (2010).
- [39] M. Girardeau, *J. Math. Phys.* **1**, 516 (1960).
- [40] T. Kinoshita, T. Wenger, and D. S. Weiss, *Science* **305**, 1125 (2004).
- [41] B. Paredes, A. Widera, V. Murg, O. Mandel, S. Fölling, I. Cirac, G. V. Shlyapnikov, T. W. Hänsch, and I. Bloch, *Nature* **429**, 277 (2004).
- [42] T. Sowiński and M. Á. García-March, *Rep. Prog. Phys.* **82**, 104401 (2019).
- [43] S. Mistakidis, G. Katsimiga, G. Koutentakis, T. Busch, and P. Schmelcher, *Phys. Rev. Lett.* **122**, 183001 (2019).
- [44] S. Mistakidis, F. Grusdt, G. Koutentakis, and P. Schmelcher, *New J. Phys.* **21**, 103026 (2019).
- [45] S. Mistakidis, A. Volosniev, N. Zinner, and P. Schmelcher, *Phys. Rev. A* **100**, 013619 (2019).
- [46] S. Mistakidis, G. Koutentakis, G. Katsimiga, T. Busch, and P. Schmelcher, *New J. Phys.* **22**, 043007 (2020).
- [47] U. Schollwöck, *Rev. Mod. Phys.* **77**, 259 (2005).
- [48] L. Cao, V. Bolsinger, S. Mistakidis, G. Koutentakis, S. Krönke, J. Schurer, and P. Schmelcher, *J. Chem. Phys.* **147**, 044106 (2017).
- [49] E. Bentine, T. Harte, K. Luksch, A. Barker, J. Mur-Petit, B. Yuen, and C. Foot, *J. Phys. B* **50**, 094002 (2017).
- [50] A. Barker, S. Sunami, D. Garrick, A. Beregi, K. Luksch, E. Bentine, and C. Foot, *J. Phys. B* **53**, 155001 (2020).
- [51] K. Keiler and P. Schmelcher, *Phys. Rev. A* **100**, 043616 (2019).
- [52] M. Pyzh and P. Schmelcher, *Phys. Rev. A* **102**, 023305 (2020).
- [53] M. Pyzh, K. Keiler, S. I. Mistakidis, and P. Schmelcher, *Entropy* **23**, 290 (2021).
- [54] T. Lee, F. Low, and D. Pines, *Phys. Rev.* **90**, 297 (1953).
- [55] T. H. Johnson, M. Bruderer, Y. Cai, S. R. Clark, W. Bao, and D. Jaksch, *EPL* **98**, 26001 (2012).
- [56] H. Moritz, T. Stöferle, M. Köhl, and T. Esslinger, *Phys. Rev. Lett.* **91**, 250402 (2003).
- [57] T. Stöferle, H. Moritz, C. Schori, M. Köhl, and T. Esslinger, *Phys. Rev. Lett.* **92**, 130403 (2004).
- [58] E. Haller, M. Gustavsson, M. J. Mark, J. G. Danzl, R. Hart, G. Pupillo, and H.-C. Nägerl, *Science* **325**, 1224 (2009).
- [59] B. Fang, G. Carleo, A. Johnson, and I. Bouchoule, *Phys. Rev. Lett.* **113**, 035301 (2014).
- [60] J. Abraham and M. Bonitz, *Contrib. to Plasma Phys.* **54**, 27 (2014).
- [61] C. McDonald, G. Orlando, J. Abraham, D. Hochstuhl, M. Bonitz, and T. Brabec, *Phys. Rev. Lett.* **111**, 256801 (2013).
- [62] G. Astrakharchik, R. Combescot, X. Leyronas, and S. Stringari, *Phys. Rev. Lett.* **95**, 030404 (2005).
- [63] A. Altmeyer, S. Riedl, C. Kohstall, M. Wright, R. Geursen, M. Bartenstein, C. Chin, J. H. Denschlag, and R. Grimm, *Phys. Rev. Lett.* **98**, 040401 (2007).
- [64] X. Andrade, J. N. Sanders, and A. Aspuru-Guzik, *PNAS* **109**, 13928 (2012).
- [65] M. Pyzh, S. Krönke, C. Weitenberg, and P. Schmelcher, *New J. Phys.* **20**, 015006 (2018).
- [66] L. Cao, S. Krönke, O. Vendrell, and P. Schmelcher, *J. Chem. Phys.* **139**, 134103 (2013).
- [67] S. Krönke, L. Cao, O. Vendrell, and P. Schmelcher, *New J. Phys.* **15**, 063018 (2013).
- [68] J. Light, I. Hamilton, and J. Lill, *J. Chem. Phys.* **82**, 1400 (1985).
- [69] A. Raab, *Chem. Phys. Lett.* **319**, 674 (2000).
- [70] E. Van Den Berg and M. P. Friedlander, *SIAM J. Sci. Comput.* **31**, 890 (2009).
- [71] I. Loris, *Comput. Phys. Commun.* **179**, 895 (2008).
- [72] R. Schmitz, S. Krönke, L. Cao, and P. Schmelcher, *Phys. Rev. A* **88**, 043601 (2013).